

# Front and Back Illuminated Dynamic and Active Pixel Vision Sensors Comparison

Gemma Taverni, *Student Member, IEEE*, Diederik Paul Moeys, *Student Member, IEEE*, Chenghan Li, Celso Cavaco, Vasyly Motsnyi, David San Segundo Bello, *Member, IEEE*, Tobi Delbruck, *Fellow, IEEE*

**Abstract**— Back Side Illumination has become standard image sensor technology owing to superior quantum efficiency and fill factor. A direct comparison of Front and Back Side Illumination (FSI and BSI) used in event-based Dynamic and Active Pixel Vision Sensors (DAVIS) is interesting because of the potential of BSI to greatly increase the small 20% fill factor of these complex pixels. This paper compares identically-designed front and back illuminated DAVIS silicon retina vision sensors. They are compared in terms of Quantum Efficiency (QE), Leak Activity (LA) and Modulation Transfer Function (MTF). The BSI DAVIS achieves a peak QE of 93% compared with the FSI DAVIS, peak QE of 24%, but reduced MTF, due to pixel crosstalk and parasitic photocurrent. Significant “leak events” in the BSI DAVIS limit its use to controlled illumination scenarios without very bright light sources. Effects of parasitic photocurrent and modulation transfer functions with and without IR cut filters are also reported.

**Index Terms**—Dynamic Vision Sensor, Event-based camera, Image sensor, Neuromorphics, Vision sensor

## I. INTRODUCTION

Event-based neuromorphic vision is an emerging field of machine vision. The Dynamic Vision Sensor (DVS) [1] has applications stemming from its high temporal resolution, low latency, high dynamic range, and sparse output. Each DVS pixel reports brightness change (log intensity change) events. The latency and amount of transferred data is reduced compared with conventional image sensors. The high dynamic range, due to the logarithmic phototransduction, allows application with less controlled lighting.

The Dynamic and Active Pixel Vision Sensor (DAVIS) [2] was introduced to add conventional static frame output to the DVS at minimal pixel area cost. The DAVIS uses an Active Pixel Sensor (APS) readout circuit that integrates the shared

photodiode current to produce gray scale intensity values. This way, the sensor concurrently detects asynchronous brightness change events while it outputs conventional gray scale images. The combination of the two sensors can be used for lens calibration, focusing, or anytime some combination of static and dynamic features are required [3].

The growing interest in DAVIS and DVS sensors has pushed the exploration of new techniques in order to reach higher performance in terms of sensitivity and low illuminance operation, so to extend applications in new fields such as fluorescent microscopy [4] and astronomy [5].

Past developments of the DAVIS aimed to reach higher DVS sensitivity using approaches mostly based on increasing the gain of the DVS front-end circuit, through the introduction of a new amplification stage [6]–[9]. A higher gain increases both the signal and the noise, while not necessarily resulting in an increase of the signal to noise ratio.

A fundamental limitation in complex pixels like the DAVIS is the achievable fill factor. Since the pixel design is complex (typically about 45 transistors), the fraction of pixel area occupied by the photodiode is limited to about 20%. We explored the use of CMOS Image Sensor (CIS) technology to increase quantum efficiency, by using microlenses and Antireflection Coating (ARC) for the Front Side Illumination (FSI) sensor, and by using Back Side Illumination (BSI) technology.

BSI enhances light sensitivity by increasing the sensitive area of the pixel [10]. Sensor illumination comes from the back of a thinned wafer, increasing the fill factor of the pixels potentially to 100% and thus improving low light performance. However, BSI is a more complex process flow and only available from some CIS foundries. BSI also introduces more pixel crosstalk and more parasitic photocurrent effects, where unintended photocurrents induced in transistor source-drain junctions cause undesirable effects.

The most important step in BSI is thinning the Si wafer to remove the non-sensitive bulk, thus to expose the photosensitive silicon epi-layer to the incoming photons. The thinning requires accurate thickness control and low surface damage that can increase surface velocity [11]–[13]. To maximize the sensitivity and minimize crosstalk, surface passivation techniques and careful substrate engineering are also important.

Manuscript submitted March 2, 2018

This work was supported in part by the European Commission projects SWITCHBOARD (H2020 Marie Curie 674901), VISUALISE (FP7-ICT-600954) and SEEBETTER (FP7-ICT-270324).

The authors G. Taverni, D. P. Moeys, C. Li and T. Delbruck are with the Institute of Neuroinformatics, University of Zurich and ETH, 8057 Zurich, Switzerland (e-mail: [getaverni@ini.uzh.ch](mailto:getaverni@ini.uzh.ch), [diederikmoeys@live.com](mailto:diederikmoeys@live.com), [lich@ini.uzh.ch](mailto:lich@ini.uzh.ch), [tobi@ini.uzh.ch](mailto:tobi@ini.uzh.ch))

The authors C. Cavaco, V. Motsnyi and D. S. Bello are with Imec research institute, 3001 Leuven, Belgium. (e-mail: [Celso.Cavaco@imec.be](mailto:Celso.Cavaco@imec.be), [Vasyly.Motsnyi@imec.be](mailto:Vasyly.Motsnyi@imec.be), [David.SanSegundoBello@imec.be](mailto:David.SanSegundoBello@imec.be))

Here we present results from two identical versions of DAVIS that differ only for the illumination side, the FSI DAVIS and BSI DAVIS. They have identical CMOS circuit design, front-end layout, and fabrication except for the bonding pads. We compare the two sensors in terms of Quantum Efficiency (QE), parasitic photocurrent effects on background “Leak Activity” (LA) noise events, and modulation transfer function (MTF).

The outline of this paper is as follows. Sec. II reviews the DAVIS chip. Sec. III describes the manufacturing. Sec. IV covers the characterization results. Sec. V concludes the paper.

## II. DAVIS

Fig. 1 shows the DVS and APS circuits [2]. The DVS part outputs a stream of brightness change events. Each event signals a change of log intensity  $\Delta \ln I_p$  exceeding a pair of temporal contrast thresholds  $\Theta_{on} > 0$  and  $\Theta_{off} < 0$ :

$$\Delta \ln I_p > \Theta_{on} \text{ or } \Delta \ln I_p < \Theta_{off} \quad (1)$$

The pixel then memorizes  $\ln I_p$  after the event is sent. The output is a variable data-rate stream of address-events consisting of the addresses of the pixels and the signs of the brightness changes. The stream is sent from the DVS interface over a digital bus that uses row and column ON and OFF request signals (RR, CRON, CROFF) and acknowledge signals (RA, CA) to provide access from the pixels to the shared digital output bus [3]. The stream is processed for applications using event-based algorithms and hardware architectures [3].

The APS readout uses transistors MN1-5 to read out the integrated signal  $V_{aps}$  with digital differential double sampling that removes the MN2 transistor offsets and some temporal noise [2]. Column select, CS, and column reset, CR, control APS readout along with the global shutter exposure stop signal TX.

The DVS switch cap amplifier is reset by the pfet switch  $M_r$ . The  $pn$  junction  $D_r$  at the  $V_{di}$  node has junction leakage  $I_{leak}$  from the nwell bulk that creates so-called ON “leak activity” [1], characterized in Hz per pixel at some specified bias and lighting condition. Increased temperature and parasitic photocurrent in the junction create additional current  $I_{par}$  that increases the leak event rate [14].  $I_{par}$  is caused by photocharge in or near  $D_r$ . In FSI DAVIS, this charge is created by light leaking through the overlying metal shielding. In BSI DAVIS it is created by light that penetrates all the way to the nwell bulk of  $M_r$ , where the resulting electrons can be collected by  $D_r$ . A main aim of this paper is to compare the effects of  $I_{par}$  in the FSI and BSI sensors. In particular, since longer wavelength light penetrates further into silicon [15], [16], we measured the effect of using IR cut filters to block Near Infrared (NIR) light.

## III. FSI AND BSI MANUFACTURING

The FSI and BSI DAVIS pixels use the same optimized buried photodiode from Towerjazz. This photodiode is a buried junction except for a small surface contact region. A deep p-type implant under all parts of the pixel aside from the photodiode builds in an electric field that pushes deep photo-

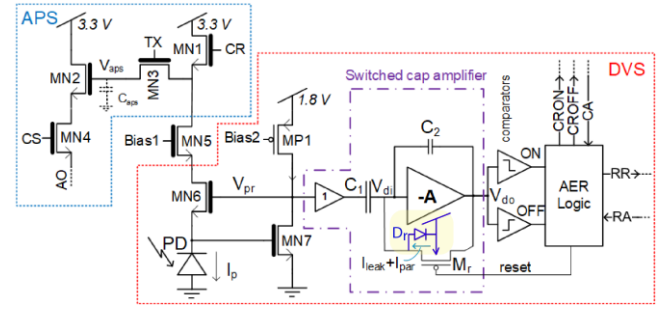


Fig. 1 Simplified DAVIS pixel circuit. Thicker gate 3.3V nfets have bold gate symbols.

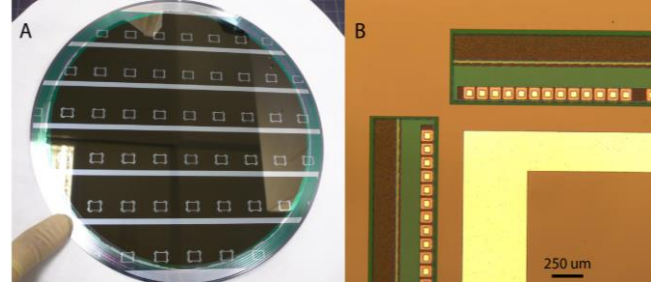


Fig. 2 BSI DAVIS wafer. **A**: Photograph of a BSI DAVIS wafer, where the aluminum pads are clearly visible. **B**: Micrograph showing the pads open from the backside for wire bonding: The silicon wafer is etched until the first metal in the pad stack is available, and then Al is deposited.

generated electrons towards the photodiode. The FSI DAVIS was processed at Towerjazz with 1um-thick 15x15  $\mu\text{m}^2$  microlenses and antireflection coating [17]. For the BSI DAVIS, fabrication was stopped after metals and passivation, i.e., before microlenses and ARC. Then the BSI wafer process flow was performed at imec.

The BSI DAVIS processing consists of the following steps [13]: bonding the original CMOS wafer front side to a carrier wafer, flipping the sensor to expose the backside, thinning the device wafer by grinding and wet etch, depositing ARC of oxide passivation, and contact opening followed by pad deposition.

The starting wafer thickness of 750  $\mu\text{m}$  was thinned until reaching the 18  $\mu\text{m}$ -thick photosensitive epi layer. Alignment marks on the CMOS allow backside bond pad opening. Bonding pads are the same as for FSI but more space was allocated between pad and core to allow for etching the trench openings to the metal1 back of the bonding pads (Fig. 2).

## IV. CHARACTERIZATION

Following the measurement procedures from [9], this paper reports only measurements which highlight the main difference between BSI and FSI DAVIS sensors. The two sensors have identical design, 18.5x18.5  $\mu\text{m}^2$  pixels, 346x260 pixel array and 22% geometrical photodiode silicon fill factor (FF).

Table I compares the main specifications of the two sensors. The previous version, DAVIS240C [2], has nearly the same pixel design but uses a simpler surface “LDD” photodiode from Towerjazz.

We characterized the two sensors in terms of quantum efficiency, leak activity, and modulation transfer function. We also studied the effect of NIR, using NIR cut filters in front of the camera with cutoff wavelengths of 750 nm, 690 nm, and 700 nm<sup>1</sup>. Longer wavelength light penetrates deeper in the substrate and affects LA, crosstalk between pixels, and modulation transfer function. Since the BSI DAVIS illuminates the back of the entire pixel, the NIR light has a larger effect on leak activity. Lighting was either from an integrating sphere with white LED<sup>2</sup> with cutoff 730 nm, Xenon lamp, halogen desk lamp, or natural sunlight.

### A. Quantum Efficiency (QE)

We did the QE measurements (Fig. 3) on a spectral response setup consisting of a uniform monochromatic narrow band light illuminating the sensor. The incident light was produced from a wide-band white light slit interferometer<sup>3</sup>. The generated photocurrents were measured from the APS frame exposure Digital Number (DN) converted to voltage by the ADC references, and then converted to charge using the measured conversion gain of about 23 uV/e<sup>-</sup>. Each measurement was compared to one from a calibrated reference photodiode to remove the effect of source spectrum.

Fig. 3 shows that BSI DAVIS has a larger QE across the spectrum, with a peak of 93% @ 390 nm. FSI DAVIS reaches a peak of 24% @ 630 nm, which is higher than the 7% peak QE of the FSI DAVIS240C, due to the introduction of buried photodiode, ARC and micro-lenses. BSI DAVIS reaches almost 100% FF. The lower QE in FSI DAVIS is due mainly to the FF of 22%, although the microlenses clearly help in focusing the light on the photodiode because the measured QE (peak at 24%) is even higher than the FF.

Both QE have a sharp cut off around 350 nm due to the borosilicate package cover glass. The BSI DAVIS has higher QE especially in the blue and UV portion of the spectrum. At shorter wavelengths, the electrons are generated in the region near the back surface and their efficiency reaches a peak of 93%. This high QE suggests that the retrograde epi doping [12] and deep p implant are very effective in steering charge to the photodiode and that the surface recombination velocity [11] at the back side is low. At longer wavelengths, charge is generated deeper within the silicon. Presumably, more of the photons generate charge above the deep p implant, and the resulting electrons are stolen by the n-wells and n source drains or recombine, resulting in a reduction of QE to 74% @ 700 nm. At longer wavelengths, this effect increases, further reducing QE. The inset in Fig. 3 plots the ratio  $QE_{BSI}/QE_{FSI}$ , and it shows how the  $QE_{BSI}$  is consistently almost 4X higher than  $QE_{FSI}$  in the visible range, while it increases even more in UV (until 10X) and reaches the lowest value for NIR (3X).

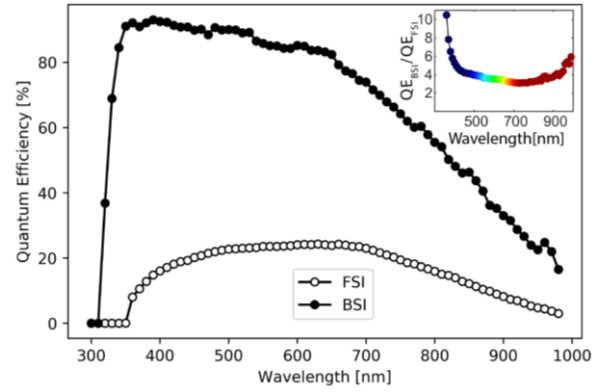


Fig. 3 Quantum Efficiency spectrum of BSI DAVIS and FSI DAVIS; (inset) QE BSI/QE FSI DAVIS ratio spectrum, the color scale represents wavelength color.

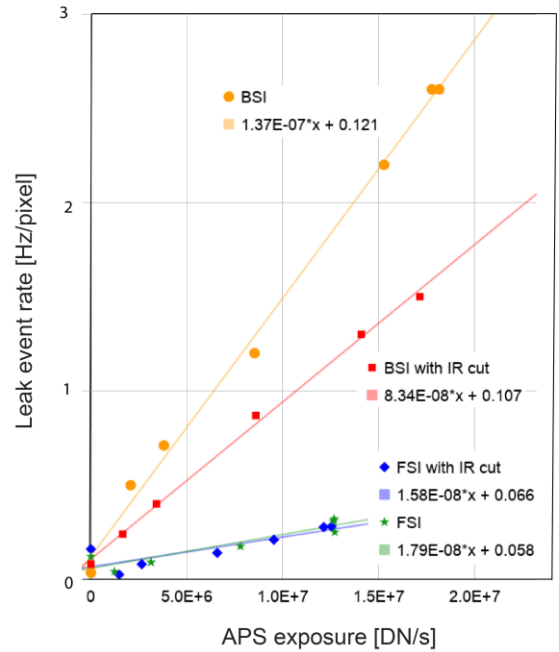


Fig. 4 Average pixel leak activity frequency of BSI and FSI DAVIS, with and without 84714 NIR cut filter using Xenon light source.

### B. Leak Activity (LA)

LA was characterized in [14] by measuring average pixel frequency of leak events  $f_{par}$  due to parasitic photocurrent in  $D_r$ . In our previous characterizations, we mistakenly measured LA using white LED lighting<sup>2</sup> which lacks NIR content. In order to investigate the effect of NIR light on the BSI DAVIS we repeated the measurements with an incandescent Xenon source light<sup>3</sup> that has significant NIR content.

During the experiments, the bias settings were left untouched. The bias currents  $I_{off} < I_d < I_{on}$  determine the event thresholds ( $I_d = 40nA$ ,  $I_{on} = 1.9uA$ ,  $I_{off} = 1.8nA$ ), while the bias current  $I_{Pr}$  and  $I_{PrSF}$  control the amplifiers in the first and second stage, determining the pixel bandwidth ( $I_{Pr} = 172pA$ ,  $I_{PrSF} = 5.3pA$ ) [14]. After biasing BSI and FSI DAVIS

<sup>1</sup> Edmund Optics IR Cut-Off Filter 49801 with cutoff 750nm, 49809 with cutoff 690nm, and 84714 with sharp cutoff at 700nm and OD>4 up to 1050nm.

<sup>2</sup> LED: CREE MHDGWT-0000-000N0UK230GCT-ND White 3000K, <http://www.cree.com/led-components/media/documents/ds-MHDG.pdf>

<sup>3</sup> Mitutoyo Xenon-based white light source

identically so that the DVS analog bandwidths and threshold were nominally the same, we verified first that under bare-chip (no lens) and fluorescent room illumination of about 300 lux, the LA was similar, with FSI at  $f_{\text{par}}=0.21$  Hz and BSI at  $f_{\text{par}}=0.61$  Hz. This result accords with the estimates computed from the  $f_{\text{par}}/\text{lux}$  from [14] of about 0.2 Hz (FSI) and 0.43 Hz (BSI). Repeating the measurements with a halogen desk lamp showed extreme difference between the two sensors: The FSI LA increased to only 0.55 Hz, but the BSI LA went to 36 Hz. Covering the BSI DAVIS with the 49801 NIR cut filter reduced BSI DAVIS LA to about 6.7 Hz but it was still more than 10X larger than for the FSI DAVIS.

We next repeated the measurements in a more controlled environment using a sharper cutoff filter NIR filter and measuring LA at different levels of illumination. We used a Xenon lamp coupled directly to an integrating sphere and imaged the sphere opening with a 6mm lens, on which we placed the 84714 NIR filter to block the significant peaks in NIR in the Xenon source past 700 nm. Fig. 4 plots LA rates versus measured light exposure. We measured exposure using the APS mode of the DAVIS, by computing the DN/s produced by the light. One DN (digital number) is about 1.5 mV, or about  $65 e^-$ .

Fig. 4 shows that all responses are linear with measured exposure. They also clearly indicate that the BSI DAVIS is much more sensitive to LA caused by both visible and especially NIR light. The FSI LA is barely affected by NIR light; its LA is reduced by only a factor of 0.88X by using the filter. On the other hand, the BSI LA is reduced by a factor of 0.61X by blocking NIR. The unfiltered BSI LA is about a factor of 7.7X larger than that of the FSI DAVIS. These results suggest that even visible light is penetrating the back wafer to create parasitic photocurrent in the switch transistor.

We did one additional experiment to refine this conclusion. To restrict the spectrum further, we placed various color filters from an Edmund science kit (761019-6) in front of the NIR filter. Without color filter, the BSI LA was 36Hz. Remarkably, including a cyan filter reduced the LA to 0.1Hz, while only reducing exposure by 6X. Thus, using a cyan filter reduces the LA per exposure by more than  $(36/.1)/6=60X$ . By contrast, a red filter only reduced the LA to 29Hz. This result clearly shows that long wavelength light is the dominant source of LA in the BSI DAVIS.

The much higher NIR-induced LA sensitivity of the BSI DAVIS means that its performance is improved when using it

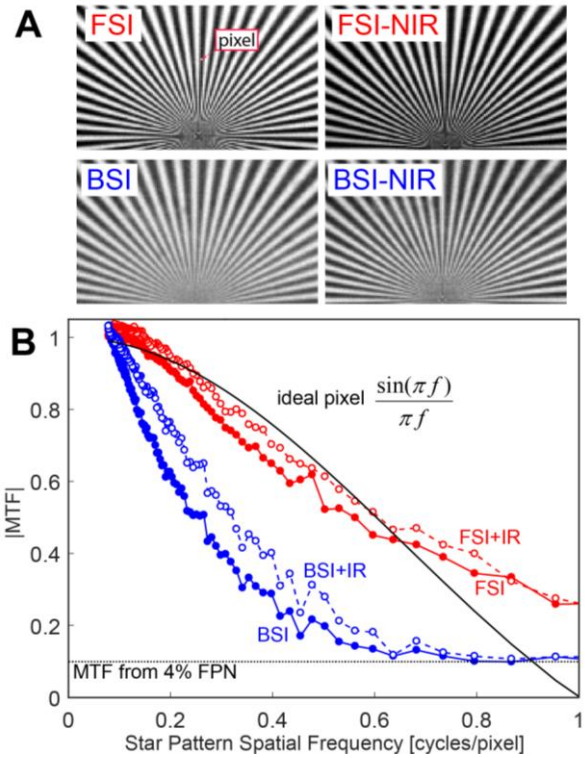


Fig. 5 Modulation transfer function measurements using 60W incandescent lighting. **A:** Images without and with IR cut filter. **B:** MTF value for spatial frequency (cycles/pixel).

with sunlight or incandescent light by including an NIR filter, perhaps combined with a red-blocking filter. Otherwise, the BSI DAVIS is thus currently not very usable in scenes with bright light sources, due to the excessive LA, unless we consider this DC response as a feature for detecting light sources.

### C. Modulation Transfer Function (MTF)

The MTF is a measure of the spatial resolution of an image sensor. We measured it as the amount of modulation of a black and white sinusoidal pattern of a particular frequency  $f$  in cycles/pixel along concentric circles, and has a maximum of 1.0. We used a modified “Siemens star chart” method described in [19]. We recorded images from BSI DAVIS and FSI DAVIS with a 16mm lens and a 60W incandescent bulb for illumination and repeated the measurements with/without the Edmund 49801 IR cut filter (Fig. 5A). APS frames show that FSI DAVIS has higher spatial resolution (Fig. 5A). BSI images take on a gray value in the center of the chart, while FSI images can resolve higher frequency lines and are visually sharper. The use of NIR filter slightly improves the resolution.

In an ideal rectangular pixel with no cross-talk the geometric MTF is  $\sin(\pi f)/\pi f$  as shown in Fig. 5B. To compute the measured MTF, we read the DN pixel values along concentric circles. Since the circumference is  $2\pi r$  pixels at radius  $r$ , and there are  $N=60$  fan segment cycles, the spatial frequency in cycles/pixel is  $f = N/2\pi r$ . The Fig. 5B MTF values are the root mean square (RMS) deviation from mean

TABLE I  
SENSOR SPECIFICATIONS

	FSI DAVIS240C[2]	FSI DAVIS (DAVIS346B)	BSI DAVIS (DAVIS346C)
Technology	180 nm 1P6M MIM CIS		
Pixel complexity	48 transistors, 2 MIM caps, 1 MOS cap		
Array size	240x180	346x260	
Pixel size $\mu\text{m}^2$	18.5x18.5		
Fill factor	22%	22%	100% (BSI)
Photodiode	Surface	Buried, surface contact	
Peak QE	7%	24%	93%

value calculated as  $2\sqrt{2}\text{RMS}$ ; the prefactor  $2\sqrt{2}$  converts from RMS to sinusoidal peak to peak amplitude. The measured MTF has maximum values slightly larger than 1 due to the local normalization method we used to remove effects of illumination and response shading. The plot shows the ideal geometric MTF, without taking in consideration the diffusion of carriers in the substrate. The addition of the diffusion MTF explain the two different shapes of BSI DAVIS and FSI DAVIS, as it can be seen in the models in [20]-[21].

The MTF results show that the FSI DAVIS has higher MTF for all spatial frequencies and is nearly ideal, i.e. there is little cross talk. Blocking NIR increases both sensor MTFs but only slightly. The BSI DAVIS MTF drops to its asymptotic value at  $f=0.5$ , suggesting that pixels average their immediate neighbors. Thus, the BSI DAVIS MTF provides intrinsic antialiasing at the cost of lower resolution. This result is consistent with the square aspect ratio of the pixel dimension (18.5 $\mu\text{m}$ ) and the epi thickness (18 $\mu\text{m}$ ). The MTF is larger than theory for high frequency because the RMS metric also measures aliasing and the ~4% pixel fixed pattern noise (FPN); an FPN of 4% (~3% of which is caused by output shading) would result in an MTF of  $(2\sqrt{2})0.04 = 0.11$ .

## V. CONCLUSION

Compared to the previous generation DAVIS240C, the FSI DAVIS has about 3.5X higher QE and the BSI DAVIS has 13X higher QE. The BSI DAVIS, with its 4X higher QE than the FSI DAVIS, has clear advantages for low light applications such as the fluorescent calcium neural imaging of [4], where the lighting spectrum can be controlled and where the lower MTF can be tolerated. However, the increased sensitivity of leak events to parasitic photocurrent caused by NIR currently limits applications of the BSI DAVIS to controlled lighting. The results point to further development of BSI DAVIS with shallower epi layer and trench isolation between pixels [13], and suggests that a pixel modification to reduce leak events such as the one proposed in [21] could be beneficial.

## ACKNOWLEDGMENT

We thank members of the Sensors Group at the Institute of Neuroinformatics, imec, inilabs, and Towerjazz. Funding was provided by the European Commission projects SWITCHBOARD (H2020 Marie Curie 674901), VISUALISE (FP7-ICT-600954) and SEEBETTER (FP7-ICT-270324).

## REFERENCES

- [1] P. Lichtsteiner, C. Posch, and T. Delbruck, "A 128 x 128 120 dB 15  $\mu\text{s}$  Latency Asynchronous Temporal Contrast Vision Sensor," *IEEE J. Solid-State Circuits*, vol. 43, no. 2, pp. 566–576, 2008.
- [2] C. Brandli, R. Berner, M. Yang, S.-C. Liu, and T. Delbruck, "A 240x180 130 dB 3  $\mu\text{s}$  Latency Global Shutter Spatiotemporal Vision Sensor," *IEEE J. Solid-State Circuits*, vol. 49, no. 10, pp. 2333–2341, Oct. 2014.
- [3] S.-C. Liu, T. Delbruck, G. Indiveri, A. Whatley, and R. Douglas, Eds., *Event-Based Neuromorphic Systems*. John Wiley and Sons Ltd., UK, 2015.
- [4] G. Taverni *et al.*, "In-vivo Imaging of Neural Activity with Dynamic Vision Sensors," in *2017 IEEE Biomedical Circuits and Systems Conference (BioCAS)*, Turin, Italy, 2017.
- [5] G. Cohen *et al.*, "Event-based Sensing for Space Situational Awareness," in *Proc. the Advanced Maui Optical and Space Surveillance Technologies Conf., (AMOS)*, Maui, Hawaii, USA, 2017.
- [6] T. Serrano-Gotarredona and B. Linares-Barranco, "A 128 x 128 1.5% Contrast Sensitivity 0.9% FPN 3  $\mu\text{s}$  Latency 4 mW Asynchronous Frame-Free Dynamic Vision Sensor Using Transimpedance Preamplifiers," *IEEE J. Solid-State Circuits*, vol. 48, no. 3, pp. 827–838, Mar. 2013.
- [7] C. Posch, D. Matolin, and R. Wohlgenannt, "A two-stage capacitive-feedback differencing amplifier for temporal contrast IR sensors," *Analog Integr. Circuits Signal Process.*, vol. 64, no. 1, pp. 45–54, Jul. 2010.
- [8] M. Yang, S.-C. Liu, and T. Delbruck, "A Dynamic Vision Sensor With 1% Temporal Contrast Sensitivity and In-Pixel Asynchronous Delta Modulator for Event Encoding," *IEEE J. Solid-State Circuits*, vol. 50, no. 9, pp. 1–12, Sep. 2015.
- [9] D. P. Moeys *et al.*, "A Sensitive Dynamic and Active Pixel Vision Sensor for Color or Neural Imaging Applications," *IEEE Trans. Biomed. Circuits Syst.*, vol. PP, no. 99, pp. 1–14, 2017.
- [10] R. Nixon, N. Doudoumopoulos, and E. R. Fossum, "Backside illumination of CMOS image sensor," US6429036 B1, 06-Aug-2002.
- [11] A. S. Grove, *Physics and Technology of Semiconductor Devices*. New York: John Wiley and Sons, Inc., 1967.
- [12] K. D. Munck, K. Minoglou, and P. D. Moor, "Thinned Backside-Illuminated (BSI) Imagers," in *Ultra-thin Chip Technology and Applications*, Springer, New York, NY, 2011, pp. 337–352.
- [13] C. Cavaco, "On the Fabrication of Backside Illuminated Image Sensors: Bonding Oxide, Edge Trimming and CMP Rework Routes," presented at the 2014 ECS and SMEQ Joint International Meeting (October 5-9, 2014), 2014.
- [14] Y. Nozaki and T. Delbruck, "Temperature and Parasitic Photocurrent Effects in Dynamic Vision Sensors," *IEEE Trans. Electron Devices*, vol. PP, no. 99, pp. 1–7, 2017.
- [15] W. C. Dash and R. Newman, "Intrinsic Optical Absorption in Single-Crystal Germanium and Silicon at 77K and 300K," *Phys. Rev.*, vol. 99, no. 4, pp. 1151–1155, Aug. 1955.
- [16] T. Delbruck and C. A. Mead, "Analog VLSI adaptive logarithmic wide-dynamic-range photoreceptor," presented at the 1994 IEEE International Symposium on Circuits and Systems, 1994, vol. 4, pp. 339–342.
- [17] B. Vereecke *et al.*, "Quantum efficiency and dark current evaluation of a backside illuminated CMOS image sensor," *Jpn. J. Appl. Phys.*, vol. 54, no. 4S, p. 04DE09, Mar. 2015.
- [18] A. Theuwissen, "How to Measure Modulation Transfer Function (1) « Harvest Imaging Blog," 20-Feb-2014. .
- [19] B. Fowler, "Solid-State Image Sensors," in *Handbook of Digital Imaging*, John Wiley & Sons, Ltd, 2015.
- [20] I. Djite, M. Estribeau, P. Magnan, G. Rolland, S. Petit, and O. Saint-Pe, "Theoretical Models of Modulation Transfer Function, Quantum Efficiency, and Crosstalk for CCD and CMOS Image Sensors," *IEEE Trans. Electron Devices*, vol. 59, no. 3, pp. 729–737, Mar. 2012.
- [21] B. Son *et al.*, "A 640x480 Dynamic Vision Sensor with a 9 $\mu\text{m}$  Pixel and 300Meps Address-Event Representation," in *2017 International Solid State Circuits Conference (ISSCC) Tech. Dig.*, San Francisco, CA, USA, p. 4.1.